Cardiopulmonary Imaging Using a High-Performance 0.55T MRI System

Adrienne E. Campbell-Washburn; Robert J. Lederman; Robert S. Balaban

Division of Intramural Research, National Heart, Lung, and Blood Institute, National Institutes of Health, Bethesda, MD, USA

NHLBI 0.55T ramped-down MRI system

New generations of lower field MRI system, equipped with modern hardware and contemporary imaging capabilities, have garnered interest within the MRI community in recent years [1]. Research has focused on improving MRI accessibility in low-resource settings, engineering new hardware solutions, making MRI more portable, and developing new clinical applications [2–6].

The National Heart, Lung, and Blood Institute (NHLBI, National Institutes of Health) have developed high-performance lower field MRI technology, with particular interest in cardiac imaging, pulmonary imaging, and MRI-guided catheterization procedures [7]. We were motivated to improve catheter device safety, and aimed to leverage modern imaging methods to retain image quality and imaging speed at the lower magnetic field strength. We collaborated with Siemens Healthineers to ramp down the 1.5T MAGNETOM Aera system located in the NHLBI catheterization laboratory from 1.5T to 0.55T. Here, we will describe our ongoing work on this system.

Cardiac catheterization device heating

Despite years of development, clinical adoption of MRI-guided cardiovascular catheterization procedures remains limited [8]. Cardiac catheterization procedures can be diagnostic, for example diagnostic pressure measurements or endomyocardial biopsy, or they can be therapeutic, for example myocardial ablation procedures. Typically, these procedures are performed under fluoroscopic or electroanatomic guidance; whereas MRI offers the advantage of improved tissue contrast and the accurate assessment of cardiac function and physiology during a procedure.

MRI-guided procedures rely on real-time imaging for navigation of devices within the vasculature and chambers of the heart. Conventionally, we use a multiplanar Cartesian bSSFP acquisition, with interactive adjustment of image contrast, slice planes, acceleration rate, and other imaging parameters. In addition, rapid acquisition and low latency reconstruction of standard image contrasts are used to provide diagnostic data to operators during the procedure.

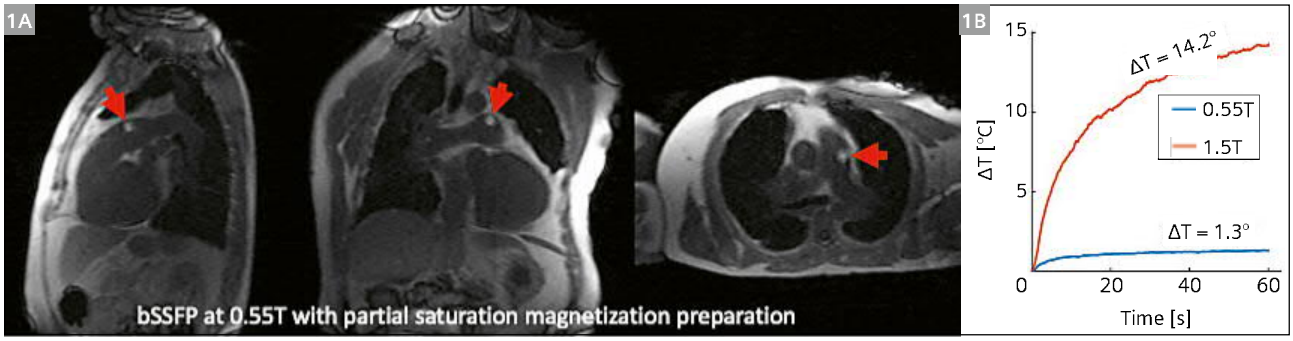

1 **(1A)** Real time bSSFP imaging with partial saturation magnetization preparation pulse used to navigate gadolinium filled balloon (red arrow) to cardiac chambers. Multiplanar imaging (three planes) is used to visualize the balloon in the main pulmonary artery. **(1B)** Temperature measured at the tip of a fully insulated guidewire (Glidewire, 180 cm x 0.035", Terumo) during real-time bSSFP imaging (TR = 2.5 ms, flip angle = 60°). Measurements are made in an ASTM2182-compliant gel phantom to generate "worst case scenario" heating [16].

Catheterization procedures rely on long metallic devices that have been carefully engineered to impart mechanical properties suitable for navigation in complex anatomy and tortuous vasculature, and with imaging properties optimized for fluoroscopy. The catheter designs are uniquely ill-suited for application in MRI due to poor visualization and RF-induced heating risking thermal injury. Nevertheless, NHLBI and other investigators have performed diagnostic catheterization procedures using polymer catheters in several hundred patients, with MRI offering invaluable diagnostic data [9–12].

To reduce concerns of RF-induced heating of devices, non-metallic devices have been proposed [13]. Unfortunately, most non-metallic alternatives have proven to be mechanically inadequate. Segmented metallic designs have also been developed to maintain mechanical properties while eliminating RF-induced heating to good effect [14]. A handful of manufacturers are developing MRI-specific devices. Still, the limited availability of MRI-safe devices remains unappealing to interventional cardiologists, who are accustomed to having numerous device options to address the idiosyncrasies of a given procedure in an individual patient.

Balancing tolerable device heating against reduced image quality, we settled on approximately 0.5T as a field strength for this application. RF power is proportional to B_0^2, meaning that for identical scan parameters, device heating is reduced by 7.5-fold at 0.55T compared with 1.5T. In addition, the standing waves that generate heating on long conductive devices have a 2.7-fold longer wavelength at 0.55T than 1.5T.

At 0.55T, we use commercially available metallic guidewires and catheters for MRI-guided diagnostic catheterization in patients, paired with standard real-time bSSFP imaging. Importantly, not all devices are inherently safe at 0.55T, and diligent safety testing is still critical. Specifically, shorter devices and devices without insulation discontinuities tend to be safer [15]. Figure 1 provides example real-time imaging during device navigation and measurements of device heating in a standard guidewire at 0.55T and 1.5T.

A more common concern during routine clinical imaging is heating of electrical leads in devices such as pacemakers, defibrillators, deep brain stimulators, and other active implants. RF-induced heating of these devices may also be reduced at lower field strength, but heating depends strongly on lead length, insulation, other properties, and additional safety testing is required to assess heating in these active implant devices.

Imaging methods for 0.55T

We sought to maintain image quality at 0.55T, even though conventional wisdom suggests SNR and associated imaging speed would be less favorable. Contemporary MRI technology is well equipped for this challenge. Clinical MRI systems use modern superconductive magnet design with excellent B_0 field homogeneity; high-performance and high-fidelity gradient subsystems; phased array coils and modern receive-chain architecture. On the other hand, both older low field MRI systems and current open-bore low field systems tend to use suboptimal magnet and gradient designs, and therefore do not benefit from these more recent hardware implementations [1]. Moreover, modern imaging methods, such as non-Cartesian data sampling, constrained reconstructions, and artificial intelligence can offer boosts in image quality that have not been applied to most low field MRI systems.

To improve image SNR, we have focused on SNR-efficient spiral and echo-planar imaging (EPI), which are amenable to lower field, as well as compressed sensing image reconstructions. Spiral and EPI imaging rely on B_0 field homogeneity and long T2 or T2* for distortion-free imaging with high SNR without increased scan time. Figure 2 provides simulations of relative SNR for T1-weighted spin echo, T2-weighted turbo spin echo, and spoiled gradient echo (without blood inflow) contrasts. These simulations assume that the sampling efficiency (ratio of data sampling time to imaging time) can increase linearly with decreasing field strength. Polarization alone predicts SNR at 0.55T is 37% of 1.5T, however both relative signal intensity and contrast are increased by using SNR-efficient readouts and optimized sequence parameters.

Using our high-performance 0.55T MRI system, we implemented spiral bSSFP for cardiac imaging with a long readout (6.5 ms) and long TR (8 ms) that would not be possible at higher field strength where B_0 inhomogeneities cause banding artifacts [18]. For identical scan time and spatiotemporal resolution, we were able to achieve 69±14% of the SNR measured at 1.5T, instead of 37% predicted by polarization alone. Figure 3 provides example images.

Compressed sensing, and other constrained image reconstruction methods, can also be applied to improve image quality and SNR with their inherent denoising properties [6]. These methods are computationally costly, however computational power is becoming steadily more affordable and accessible, including through cloud resources in regions with stable internet connectivity. At 0.55T, we have applied ℓ1-SPIRiT image reconstruction for cardiac imaging. This image reconstruction is implemented using Gadgetron image reconstruction framework (https://github.com/gadgetron) [19] deployed on the

Microsoft Azure Cloud, such that reconstruction can be parallelized over multiple nodes [20]. Figure 4 demonstrates this method at 0.55T and 1.5T on the same patient [21]. Higher flip angle used at 0.55T suppresses the myocardium signal resulting in different image contrast, otherwise the two images are nearly indistinguishable.

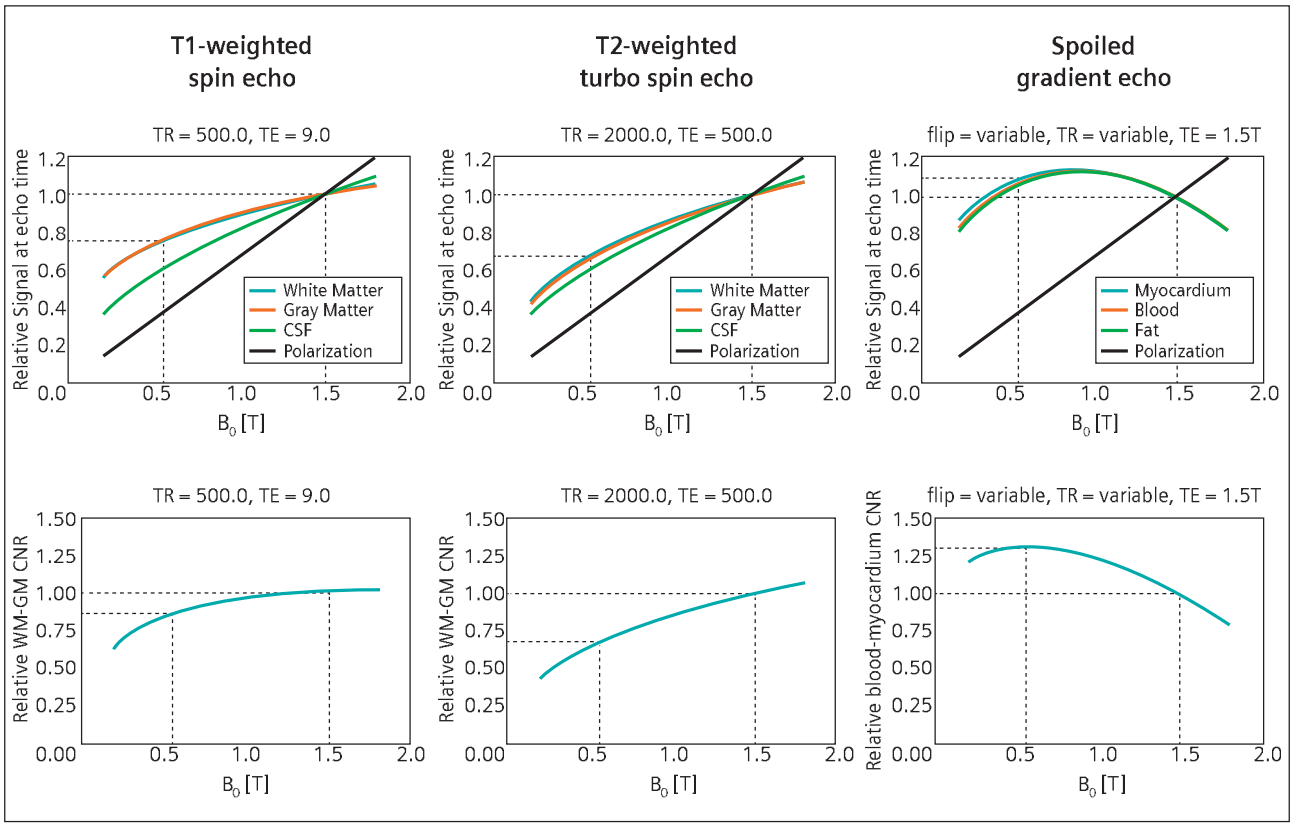

2 Bloch equation simulations of relative signal (top row) and relative contrast (bottom row) across field strengths for T1-weighted spin echo neuroimaging, T2-weighted turbo spin echo neuroimaging, and spoiled gradient echo cardiac imaging. T1 and T2 values were approximated using Bottomley et al. [17]. Blood inflow was not simulated here, which alters contrast, especially in spoiled gradient echo imaging. Both relative signal intensity and contrast are higher than expected from polarization alone.

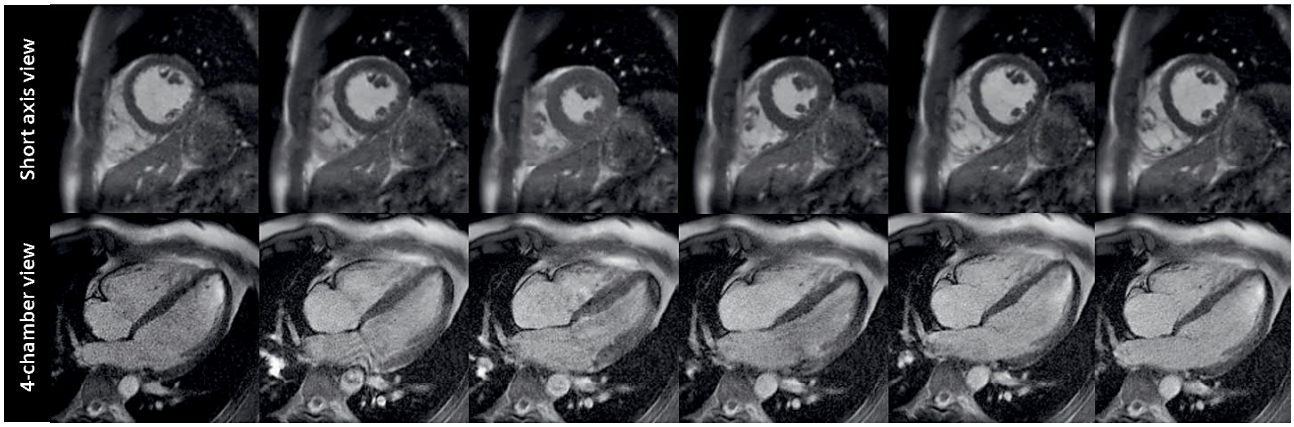

3 Spiral bSSFP cine imaging displayed during multiple frames of the cardiac cycle. Spiral bSSFP was implemented at 0.55T to exploit the uniform B_0 field (spiral readout = 6.5 ms, TR = 8 ms) for improved SNR.

Pulmonary imaging at 0.55T

Lung parenchyma imaging had been largely ineffective at 1.5T because of air-tissue interfaces causing susceptibility gradient artifacts. However, high-performance low field MRI enables high quality pulmonary imaging and combined cardiopulmonary assessment in the MRI-catheterization environment. By virtue of the improved B_0, using the contemporary magnet design employed in our prototype system, proton imaging of the lung parenchyma is possible. Figure 5 provides example T2-weighted MRI images compared with CT. MRI uses lower spatial resolution, but provides comparable information content in the lung parenchyma.

The primary benefit of MR imaging for pulmonary applications is measurement of regional function and tissue characterization information, which are beyond the scope of a clinical CT scanner [22]. Serendipitously, oxygen exhibits increased relaxivity at lower field strengths, and may enable functional oxygen-enhanced pulmonary imaging [23]. Fourier-decomposition techniques and hyperpolarized gas methods are also of interest. In addition, tissue characterization via the flexible image contrast of MRI is feasible at 0.55T where parenchymal imaging is possible.

The importance of structural and functional lung imaging has been emphasized during the recent COVID-19 pandemic, and we hope that MRI systems optimized for pulmonary imaging will be valuable for this application in the future.

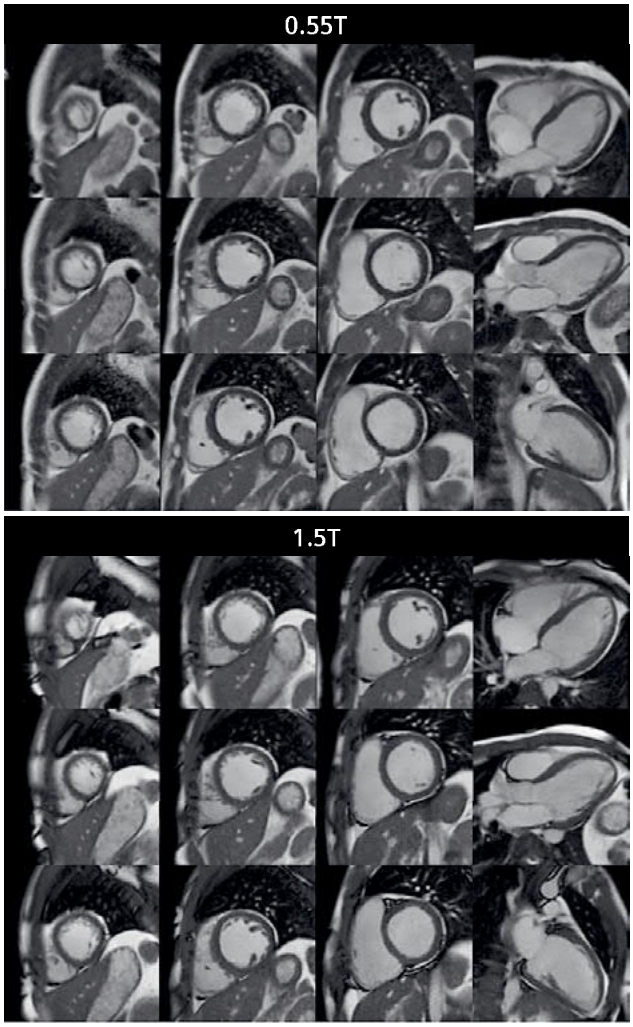

4 Free-breathing motion corrected re-binned cardiac cine imaging acquired in the same patient at 0.55T and 1.5T. Image reconstruction is performed using compressed sensing. Image quality is recovered via the compressed sensing reconstruction such that imaging from two field strengths is nearly indistinguishable.

Summary

With mature MRI hardware and sophisticated imaging methods, it is timely to revisit what is possible at lower field, both for existing clinical applications, and for new clinical applications. Contrast agent performance, image acquisition methods, image reconstruction methods, integration of new AI technology, applications in high-susceptibility regions, dynamic imaging applications, MRI-guided interventional procedures, and more, are ripe for exploration.

Disclaimer

The views and opinions of Drs. Campbell, Lederman, and Balaban expressed in this publication are based on research performed under a Cooperative Research and Development

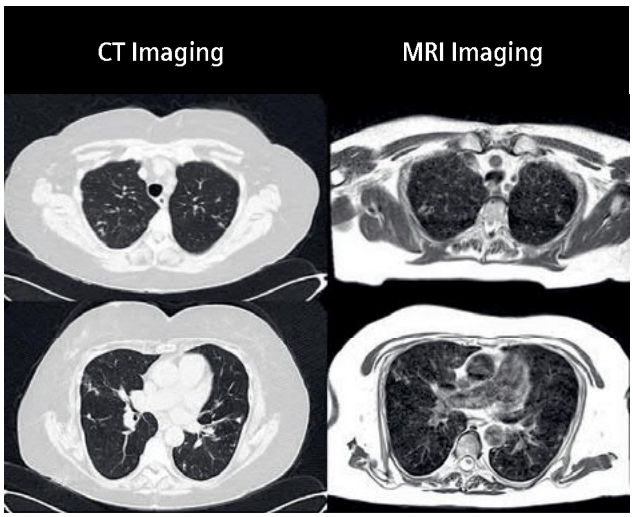

5 Comparison of CT images (2 mm slices, 0.8 x 0.8 mm in-plane resolution) to T2-weighted TSE MRI (6 mm slices, 1.2 x 1.2 mm in-plane resolution) in a patient with bronchiectasis, tree-in-bud and reticular opacities. Two difference slices are displayed. Lung parenchymal well visualized by using high-performance 0.55T MRI.

Agreement (CRADA) between Siemens Healthineers and National Heart, Lung, and Blood Institute (NHLBI), an institute of the National Institutes of Health (NIH). Neither NIH, NHLBI, nor its employees directly or indirectly endorse any product or service that is or will be provided by Siemens Healthineers or its affiliates. Siemens Healthineers acknowledges and agrees that the views and opinions of Drs. Campbell, Lederman, and Balaban expressed herein do not in any way state or imply that the U.S. Government or any of its organizational units or employees endorses any product or service of Siemens Healthineers or its affiliates.

Financial support

This work was supported by the Division of Intramural Research, National Heart, Lung, and Blood Institute, National Institutes of Health.

Acknowledgments

We thank the team at the NIH, including the MRI Technology Program, the Laboratory of Cardiovascular Intervention, the Medical Image and Signal Processing Program, and the Cardiovascular CT Program, for their work on this system. We also acknowledge Siemens Healthineers for their assistance in the modification of the MRI system for operation at 0.55T under an existing cooperative research agreement (CRADA) between NHLBI and Siemens Healthcare.

References

1 Marques JP, Simonis FFJ, Webb AG. Low-field MRI: An MR physics perspective. J Magn Reson Imaging. 2019;49(6):1528-42.
2 Sarracanie M, LaPierre CD, Salameh N, Waddington DEJ, Witzel T, Rosen MS. Low-Cost High-Performance MRI. Sci Rep. 2015;5:15177.
3 Tsai LL, Mair RW, Rosen MS, Patz S, Walsworth RL. An open-access, very-low-field MRI system for posture-dependent 3He human lung imaging. J Magn Reson. 2008;193(2):274-85.
4 Cooley CZ, Haskell MW, Cauley SF, Sappo C, Lapierre CD, Ha CG, et al. Design of sparse Halbach magnet arrays for portable MRI using a genetic algorithm. IEEE Trans Magn. 2018;54(1).
5 O'Reilly T, Teeuwisse WM, Webb AG. Three-dimensional MRI in a homogenous 27cm diameter bore Halbach array magnet. J Magn Reson. 2019;307:106578.
6 Simonetti OP, Ahmad R. Low-Field Cardiac Magnetic Resonance Imaging: A Compelling Case for Cardiac Magnetic Resonance's Future. Circ Cardiovasc Imaging. 2017;10(6).
7 Campbell-Washburn AE, Ramasawmy R, Restivo MC, Bhattacharya I, Basar B, Herzka DA, et al. Opportunities in Interventional and Diagnostic Imaging by Using High-performance Low-Field-Strength MRI. Radiology. 2019:190452.
8 Rogers T, Lederman RJ. Interventional CMR: Clinical Applications and Future Directions. Curr Cardiol Rep. 2015;17(5):580.
9 Rogers T, Ratnayaka K, Khan JM, Stine A, Schenke WH, Grant LP, et al. CMR fluoroscopy right heart catheterization for cardiac output and pulmonary vascular resistance: results in 102 patients. J Cardiovasc Magn Reson. 2017;19(1):54.
10 Ratnayaka K, Kanter JP, Faranesh AZ, Grant EK, Olivieri LJ, Cross RR, et al. Radiation-free CMR diagnostic heart catheterization in children. J Cardiovasc Magn Reson. 2017;19(1):65.
11 Pushparajah K, Tzifa A, Razavi R. Cardiac MRI catheterization: a 10-year single institution experience and review. Interventional Cardiology. 2014;6(3).
12 Knight DS, Kotecha T, Martinez-Naharro A, Brown JT, Bertelli M, Fontana M, et al. Cardiovascular magnetic resonance-guided right heart catheterization in a conventional CMR environment - predictors of procedure success and duration in pulmonary artery hypertension. J Cardiovasc Magn Reson. 2019;21(1):57.
13 Massmann A, Buecker A, Schneider GK. Glass-Fiber-based MR-safe Guidewire for MR Imaging-guided Endovascular Interventions: In Vitro and Preclinical in Vivo Feasibility Study. Radiology. 2017;284(2):541-51.
14 Yildirim KD, Basar B, Campbell-Washburn AE, Herzka DA, Kocaturk O, Lederman RJ. A cardiovascular magnetic resonance (CMR) safe metal braided catheter design for interventional CMR at 1.5 T: freedom from radiofrequency induced heating and preserved mechanical performance. J Cardiovasc Magn Reson. 2019;21(1):16.
15 Campbell-Washburn AE, Rogers T, Stine AM, Khan JM, Ramasawmy R, Schenke WH, et al. Right heart catheterization using metallic guidewires and low SAR cardiovascular magnetic resonance fluoroscopy at 1.5 Tesla: first in human experience. J Cardiovasc Magn Reson. 2018;20(1):41.
16 ASTM. F2182-09 Standard Test Method for Measurement of Radio Frequency Induced Heating On or Near Passive Implants During Magnetic Resonance Imaging. 2009.
17 Bottomley PA, Foster TH, Argersinger RE, Pfeifer LM. A review of normal tissue hydrogen NMR relaxation times and relaxation mechanisms from 1-100 MHz: dependence on tissue type, NMR frequency, temperature, species, excision, and age. Med Phys. 1984;11(4):425-48.
18 Restivo MC, Ramasawmy R, Bandettini WP, Herzka DA, Campbell-Washburn AE. Efficient spiral in-out and EPI balanced steady-state free precession cine imaging using a high-performance 0.55T MRI. Magn Reson Med. 2020.
19 Hansen MS, Sørensen TS. Gadgetron: an open source framework for medical image reconstruction. Magn Reson Med. 2013;69(6):1768-76.
20 Xue H, Inati S, Sorensen TS, Kellman P, Hansen MS. Distributed MRI reconstruction using Gadgetron-based cloud computing. Magn Reson Med. 2015;73(3):1015-25.
21 Bandettini WP, Shanbhag SM, Mancini C, McGuirt DR, Kellman P, Xue H, et al. A comparison of cine CMR imaging at 0.55 T and 1.5 T. J Cardiovasc Magn Reson. 2020;22(1):37.
22 Campbell-Washburn AE. 2019 ATS BEAR Cage Winning Proposal: Lung Imaging Using High-performance Low-field MRI. Am J Respir Crit Care Med. 2020.
23 Mirhej ME. Proton Spin Relaxation By Paramagnetic Molecular Oxygen. Canadian Journal of Chemistry. 1965;43(5):1130-8.

Contact

Adrienne E Campbell-Washburn, Ph.D.
National Heart, Lung,
and Blood Institute
National Institutes of Health
10 Center Dr., Building 10 Rm B1D47
Bethesda MD, 20892
USA
adrienne.campbell@nih.gov